Modeling of Cyclic Ratchetting Plasticity, Part II: Comparison of Model Simulations With Experiments

Y. Jiang[1]
Research Assistant.

H. Sehitoglu
Professor.

Department of Mechanical and Industrial Engineering,
University of Illinois at Urbana-Champaign,
1206 W. Green Street,
Urbana, IL 61801

The material constants of the new plasticity model proposed in the first part of the paper can be divided into two independent groups. The first group, $c^{(i)}$ and $r^{(i)}$ ($i = 1, 2, \ldots, M$), describes balanced loading and the second group, $\chi^{(i)}$ ($i = 1, 2, \ldots, M$), characterizes unbalanced loading. We define balanced loading as the case when a virgin material initially isotropic will undergo no ratchetting and/or mean stress relaxation, and unbalanced loading as the loading under which a virgin material initially isotropic will produce strain ratchetting and/or mean stress relaxation. The independence of the two groups of material constants and the interpretation of the model with a limiting surface concept facilitated the determination of material constants. We describe in detail a computational procedure to determine the material constants in the models from simple uniaxial experiments. The theoretical predictions obtained by using the new plasticity model are compared with a number of multiple step ratchetting experiments under both uniaxial and biaxial tension-torsion loading. In multiple step experiments, the mean stress and stress amplitude are varied in a stepwise fashion during the test. Very close agreements are achieved between the experimental results and the model simulations including cases of nonproportional loading. Specifically, the new model predicted long-term ratchetting rate decay more accurately than the previous models.

1 Determination of Material Constants for the New Model

In this paper, a method of establishing the material constants for the proposed model will be described, followed by direct comparison of the simulations with the experiments. The material used was a 1070 (0.7 percent carbon) steel with a pearlitic structure. For the sake of conciseness, references listed in Part I will be used but not repeated in this part, and the notation used here is consistent with Part I.

1.1 Specialization of Hardening Rule to Uniaxial Loading. In this section, we present a rather unique procedure for determining the material constants for the constitutive model outlined in Part I.

When analyzing a uniaxial tension-compression test, consider that the uniaxial loading begins from the most compressive stress state where all the backstresses are saturated (on the limiting surfaces) in the compressive direction. Consideration of the one-dimensional problem results in the following simplifications:

$$\|\boldsymbol{\alpha}^{(i)}\| = \sqrt{\tfrac{3}{2}}|\alpha_{11}^{(i)}|; \quad n_{11} = \sqrt{\tfrac{2}{3}}; \quad dp = \sqrt{\tfrac{3}{2}}d(\Delta\epsilon^p). \tag{1}$$

$\Delta\epsilon^p$ in Eq. (1) is the axial plastic strain range measured from the strain state corresponding to the most compressive stress state. Simplifying the hardening rule for the one-dimensional problem, we have the following differential equation:

$$\frac{dy}{dx} = 1 - |y|^m y \tag{2}$$

where

$$x = \sqrt{\tfrac{3}{2}}c^{(i)}\Delta\epsilon^p; \quad y = \frac{\sqrt{\frac{3}{2}}\alpha_{11}^{(i)}}{r^{(i)}}; \quad \text{and} \quad m = \chi^{(i)}. \tag{3}$$

The initial condition corresponding to the most compressive stress state is $\alpha_{11}^{(i)} = -\sqrt{\frac{2}{3}}r^{(i)}$, $\Delta\epsilon^p = 0$, $y|_{x=0} = -1$. The solution to Eq. (2) corresponding to $m = 0$, 2, and $+\infty$ are shown in Fig. 1. We note from Fig. 1 that all solutions to Eq. (2) are asymptotic to $y = 1$ and they do not have a strong dependence on the exponent m or $\chi^{(i)}$. The asymptotic curve in Fig. 1 represents a limiting surface for the one-dimensional problem such that

$$\frac{\|\boldsymbol{\alpha}^{(i)}\|}{r^{(i)}} = 1 \quad \text{when} \quad \sqrt{\tfrac{3}{2}}c^{(i)}\Delta\epsilon_{(i)}^p = 2 \quad (i = 1, 2, \ldots, M), \tag{4}$$

where $\Delta\epsilon_{(i)}^p$ is the plastic strain range at which the ith backstress $\boldsymbol{\alpha}^{(i)}$ is saturated. This relationship will be vital when attempting to determine $c^{(i)}$ and $r^{(i)}$ in subsequent discussions.

While $c^{(i)}$ ($i = 1, 2, \ldots, M$) and k, the yield stress, may be used as variables to model transient behavior, it is assumed that they remain constant for a given reversal. Assume that $\chi^{(i)}$ ($i = 1, 2, \ldots, M$) are infinitely large, then

$$\left(\frac{\|\boldsymbol{\alpha}^{(i)}\|}{r^{(i)}}\right)^{\chi^{(i)}+1} = \begin{cases} 0 & \text{when} \quad |\boldsymbol{\alpha}^{(i)}| < r^{(i)} \\ 1 & \text{when} \quad |\boldsymbol{\alpha}^{(i)}| = r^{(i)} \end{cases} \tag{5}$$

where $\|\boldsymbol{\alpha}^{(i)}\| = r^{(i)}$ infers saturation of the ith backstress $\boldsymbol{\alpha}^{(i)}$. Since $\chi^{(i)}$ have the most pronounced influence on ratchetting

[1] Current address: Department of Mechanical Engineering, University of Reno, Reno, NV 89557.

Contributed by the Applied Mechanics Division of THE AMERICAN SOCIETY OF MECHANICAL ENGINEERS for publication in the ASME JOURNAL OF APPLIED MECHANICS.

Discussion on this paper should be addressed to the Technical Editor, Professor Lewis T. Wheeler, Department of Mechanical Engineering, University of Houston, Houston, TX 77204-4792, and will be accepted until four months after final publication of the paper itself in the ASME JOURNAL OF APPLIED MECHANICS.

Manuscript received by the ASME Applied Mechanics Division, June 20, 1994; final revision, Apr. 28, 1995. Associate Technical Editor: W. N. Sharpe, Jr.

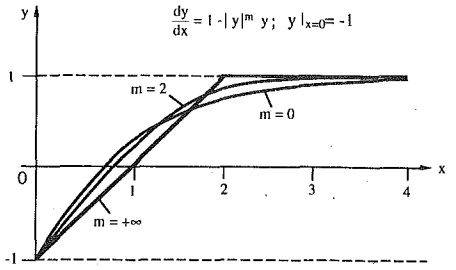

Fig. 1 Numerical solutions to the differential equation

(to be shown later), the assignment for $\chi^{(i)}$ a large number has minimal effect on the values of the constants, $c^{(i)}$ and $r^{(i)}$ (i = 1, 2, ... M). The major implication of this choice is that the uniaxial stress-strain curve simulated is piecewise linear. The plastic modulus function, when only the backstresses, j = 1, 2, ..., $(i-2)$, $(i-1)$, are saturated, can be expressed in the following form:

$$h_{(i)} = \sum_{j=i}^{M} c^{(j)} r^{(j)}. \tag{6}$$

The scalar $h_{(i)}$ represents the value of the plastic modulus function between the intervals corresponding to points $i-1$ and i.

1.2 Determination of $r^{(i)}$ from Preselected $c^{(i)}$. For the moment, if we neglect cyclic hardening and take $c^{(i)}$ (i = 1, 2, ... M) as constant, a simple procedure can be proposed to calculate the constants $c^{(i)}$ and $r^{(i)}$ (i = 1, 2, ... M) as follows. Select M points in the $\Delta\sigma - \Delta\epsilon^p$ curve from the uniaxial test (refer to Fig. 2) so that the stress range, $\Delta\sigma_{(i)}$, and plastic strain range, $\Delta\epsilon^p_{(i)}$, are known for any point i. Note that again $\Delta\epsilon^p_{(i)}$ denotes the plastic strain range at which the ith backstress $\boldsymbol{\alpha}^{(i)}$ is saturated, and $\Delta\sigma_{(i)}$ is the stress range corresponding to $\Delta\epsilon^p_{(i)}$. From Eq. (4) it follows that

$$c^{(i)} = 2\sqrt{\frac{3}{2}}\frac{1}{\Delta\epsilon^p_{(i)}} \quad (i = 1, 2, \ldots, M). \tag{7}$$

Utilizing the results of Eq. (6), the radius of the ith limiting surface can be computed as follows:

$$r^{(i)} = \frac{2}{3}\frac{H_{(i)} - H_{(i+1)}}{c^{(i)}} \quad (i = 1, 2, \ldots, M), \tag{8}$$

where

$$H_{(i)} = \frac{\Delta\sigma_{(i)} - \Delta\sigma_{(i-1)}}{\Delta\epsilon^p_{(i)} - \Delta\epsilon^p_{(i-1)}} \quad (i = 1, 2, \ldots, M), \tag{9}$$

$$\Delta\sigma_{(0)} = 2\sqrt{3}k, \quad \Delta\epsilon^p_{(0)} = 0, \quad H_{(M+1)} = 0. \tag{10}$$

The constant k is the yield stress in pure shear and the maximum stress range, $\Delta\sigma_{(M)}$, satisfies the following condition:

$$\Delta\sigma_{(M)} = 2\sqrt{\frac{3}{2}}\sum_{i=1}^{M} r^{(i)} + 2\sqrt{3}k. \tag{11}$$

$\Delta\sigma_{(M)}$ is the maximum stress range that the model is intended to simulate. The procedure (Eqs. (7)–(9)) is repeated until all $c^{(i)}$ and $r^{(i)}$ (i = 1, 2, ..., M) are determined.

Within the context used to derive the current model, the cyclic hardening is considered through the coefficients $c^{(i)}$ (i = 1, 2, ..., M) as functions of the accumulated plastic strain while the radii of the limiting surfaces, $r^{(i)}$ (i = 1, 2, ..., M), are assumed to be constants.

1.3 Determination of $c^{(i)}$ from Preselected $r^{(i)}$. When considering cyclic hardening, the method of determining $c^{(i)}$ and $r^{(i)}$ (i = 1, 2, ..., M) is somewhat more complex but we will demonstrate this as follows. If a maximum stress range is given and the yield stress has been determined, $\sum_{i=1}^{M} r^{(i)}$ can be obtained from Eq. (11) and therefore individual $r^{(i)}$ can be selected. The strategy is to find the stress and plastic strain ranges at each point in the stress-strain curve where the corresponding backstress is saturated. This procedure begins from point M and follows the order M-1, M-2, ..., 1, 0. To determine the coefficients at $(i-1)$th point (knowing ith point) the slope of the line linking the point $(i-1)$ and point i in the stress-strain reversal is calculated using the following formula:

$$H_{(i)} = \frac{3}{2}\sum_{j=i}^{M} c^{(j)} r^{(j)}. \tag{12}$$

This segment of the stress-strain curve is modeled as piecewise linear and can be described by

$$\Delta\sigma = \Delta\sigma_{(i)} + H_{(i)}(\Delta\epsilon^p - \Delta\epsilon^p_{(i)}) \quad (i = 1, 2, \ldots, M). \tag{13}$$

Point $(i-1)$ is one of the piecewise linear segment points that intersects the experimental stress-plastic strain curve, $\Delta\sigma = f(\Delta\epsilon^p)$ (Fig. 2). Once the coordinates at point $(i-1)$ are obtained, $c^{(i-1)}$ is calculated employing Eq. (7) for a known $\Delta\epsilon^p_{(i-1)}$. This procedure is repeated until all M segments have been calculated. Corresponding to a given cycle all the constants $c^{(i)}$ (i = 1, 2, ..., M) can be determined. These $c^{(i)}$ (i = 1, 2, ..., M) are plotted against p, the accumulated plastic strain, and then the relationship between $c^{(i)}$ (i = 1, 2, ..., M) and p can be established. From the $c^{(i)} - p$ (i = 1, 2, ..., M) relations, the constants $a_1^{(i)}$, $a_2^{(i)}$, $b_1^{(i)}$, and $b_2^{(i)}$ can be determined through a best fit technique. When only cyclic hardening or softening is considered, the constants $a_2^{(i)}$ and $b_2^{(i)}$ (i = 1, 2, ..., M) can be set to zero and the fitting technique can be simplified.

We note that McDowell (1992) proposed a similar procedure earlier. In McDowell's method, it was implied that only one backstress part (say ith) is active while the other parts are either saturated (backstress parts less than i) or zero (backstress parts larger than i) for fully reversed uniaxial loading. It is true that when ith backstress part is active, the backstress parts $\boldsymbol{\alpha}^{(j)}$ (j = 1, 2, ..., i-1) are saturated when $\chi^{(i)}$ are large numbers. However, the backstress parts $\boldsymbol{\alpha}^{(j)}$ ($j = i+1, i+2, \ldots, M$) are not zero.

1.4 Non-Masing Behavior. The non-Masing behavior is handled through the yield stress k as a function of the memory surface size, R_M. By conducting fully reversed strain-controlled uniaxial experiments at different strain amplitudes, the k-R_M relationship can be established. A clever way to establish this is by conducting an increasing/decreasing loading step test on a single specimen. In each step, the number of the loading cycles should be large enough so that the stress-strain responses stabilize. Because the non-Masing behavior is characterized by an increase in yield stress for a larger stress level, a shift of the hysteresis loops when putting the upper branches together allows determination of the change in yield stress for different stress levels. For uniaxial loading the following equation applies:

$$R_M = \sqrt{\frac{3}{2}}(\sigma_{\max} - \sqrt{3}k), \tag{14}$$

where $\sigma_{\max}$ is the maximum stress in the stabilized stress-strain hysteresis loop. From several selected stress/strain levels and their associated values of k, the k-R_M relationship can be established. The constants, k_0, a_k, and b_k, can be obtained using a best fit technique.

1.5 Memory Surface. Consider two steps from a decreasing step test. Since the stress amplitude in the second step is smaller than that of the first step, during the second step loading,

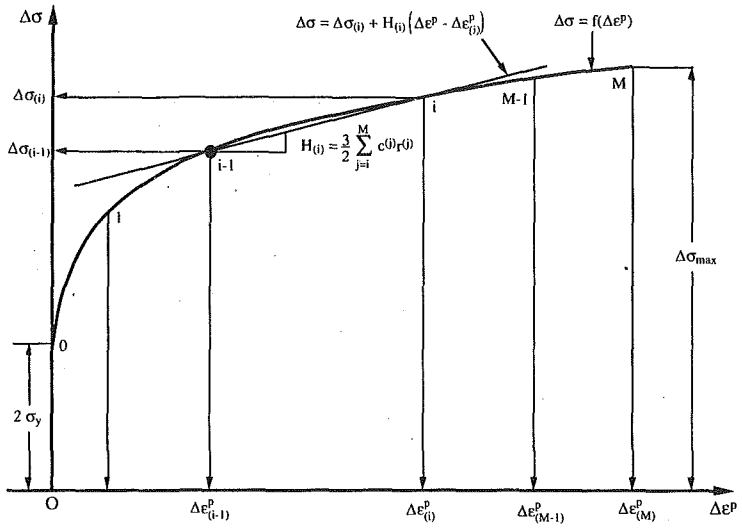

Fig. 2 Illustration of the procedure to determine $c^{(i)}$ and $r^{(i)}$ from a uniaxial stress-plastic strain reversal

$H(g) = 0$, and $|\alpha| \leq R_M$. Integrating dR_M expression results in

$$R_M = R_{M0} - c_M \int_0^{\Delta p} \left(1 - \frac{\|\alpha\|}{R_M}\right) dp, \qquad (15)$$

where Δp is the accumulated plastic strain with reference to the beginning of the second loading step. R_{M0} is the stabilized memory surface size from the first step. It is assumed that during the second loading step, there is no more cyclic hardening/softening behavior. Therefore, any change in the stress response is attributed to changes in the yield strength which are related to changes in the size of the memory surface, R_M. The instantaneous memory surface size, R_M, is calculated using Eq. (15). The constant c_M can be then determined by the trial and error fitting of R_M-Δp relation.

1.6 Determination of Exponent $\chi^{(i)}$. At this point all constants for the new model except $\chi^{(i)}$ ($i = 1, 2, \ldots, M$) have been established. The exponents $\chi^{(i)}$ ($i = 1, 2, \ldots, M$) are determined from ratchetting tests. For a given stress level, the memory surface size, R_M, is a constant, and hence $\chi^{(i)}$ is a constant. The coefficients $\chi^{(i)}$ ($i = 1, 2, \ldots, M$) can be determined from a uniaxial ratchetting test for a given stress range and mean stress. A change in the range and/or mean stress will alter the coefficients $\chi^{(i)}$ ($i = 1, 2, \ldots, M$). Using the coefficients $\chi^{(i)}$ ($i = 1, 2, \ldots, M$) obtained for several different one-step tests at different stress levels, the constants $\chi_0^{(i)}$, a_χ, and b_χ can be determined using trial and error fitting.

1.7 Discussion of the Model Constants. The model constants for 1070 Steel are given in Table 1. The determination of the material constants $c^{(i)}$ and $r^{(i)}$ ($i = 1, 2, \ldots, M$) was based on the assumption that the exponents $\chi^{(i)}$ ($i = 1, 2, \ldots, M$) were large enough so that the plastic modulus function can be treated as a step function in terms of the plastic strain. In fact, the exponents $\chi^{(i)}$ ($i = 1, 2, \ldots, M$) have little influence on the stress-strain prediction for fully reversed tension-compression. Figure 3 proves this point with simulations using the new model for $\chi^{(i)} = 0$ and $\chi^{(i)} = +\infty$ ($i = 1, 2, \ldots, M$) along with the experimental result. When $\chi^{(i)} = 0$ ($i = 1, 2, \ldots, M$), the predicted stress-strain loop is smooth. In either case, the stress-strain simulations obtained by using the new plasticity model are in close agreement with the experimental data. Therefore, the material constants $c^{(i)}$ and $r^{(i)}$ ($i = 1, 2, \ldots, M$) can be determined following the procedures introduced previously. Further analyses indicate that the exponents $\chi^{(i)}$ ($i = 1, 2, \ldots, M$) have minimal influence on the predicted results for balanced loading. As will be discussed in the next section, it is unbalanced loading where the exponents $\chi^{(i)}$ ($i = 1, 2, \ldots, M$) play an important role. This suggests that the materials constants involved in the new plasticity model can be divided into two independent groups. One group, $c^{(i)}$ and $r^{(i)}$ ($i = 1, 2, \ldots, M$), describe balanced loading and the other group, $\chi^{(i)}$ ($i = 1, 2, \ldots, M$), characterizes unbalanced loading. The independence of the two groups of material constants facilitates the determination of material constants. In view of the common features associated with the Armstrong-Frederick type models, the procedures outlined above for determining the material con-

Table 1 Material constants used in the new plasticity model for 1070 steel ($M = 10$)

$c^{(i)}$	$c_0^{(1)} = 1510$ $c_0^{(2)} = 461$ $c_0^{(3)} = 177$ $c_0^{(4)} = 77$ $c_0^{(5)} = 39$ $c_0^{(6)} = 20$ $c_0^{(7)} = 12$ $c_0^{(8)} = 6.7$ $c_0^{(9)} = 4.8$ $c_0^{(10)} = 2.7$ $a_1^{(i)} = a_2^{(i)} = 0$ (i=1, 2, ..., 10)
$r^{(i)}$	$r^{(1)} = r^{(2)} = r^{(3)} = r^{(4)} = r^{(5)} = r^{(6)} = r^{(7)} = r^{(8)} = r^{(9)} = 63.5$ MPa $r^{(10)} = 245$MPa
$\chi^{(i)}$	$a_\chi = 0.0293$ $b_\chi = 0.0128$ MPa^{-1} $Q_0^{(1)} = 0.25$ $Q_0^{(2)} = 1.0$ $Q_0^{(3)} = Q_0^{(4)} = 2.3$ $Q_0^{(5)} = Q_0^{(6)} = Q_0^{(7)} = Q_0^{(8)} = Q_0^{(9)} = 2.75$ $Q_0^{(10)} = 4.5$
Others	$c_M = 10$ $k_1 = 92.7$ MPa $a_k = 0.0361$ $c_k = 0.0094$ MPa^{-1}

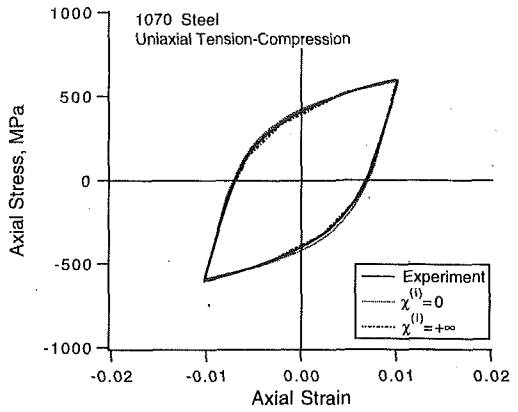

Fig. 3 Demonstration of the minimal influence of $\chi^{(i)}$ on the stress-strain description of a uniaxial balanced loading

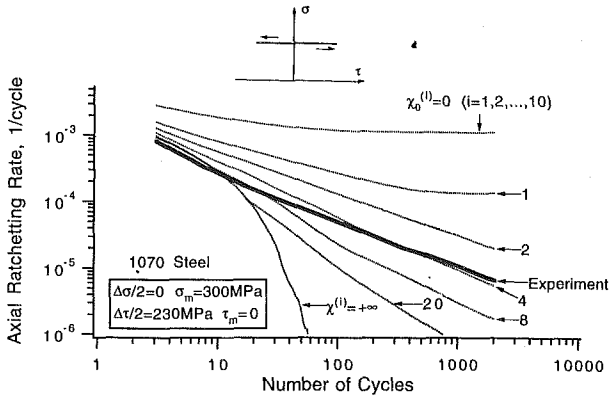

Fig. 5 Relationship between $\chi^{(i)}$ and ratchetting rate predicted by the new model for nonproportional axial-torsion consisting of alternating shear with constant axial stress

stants can be also applied to the original Armstrong-Frederick model (1966), the model of Chaboche et al. (1979), and the Ohno-Wang model (1993).

2 Experimental Procedure and Simulations

The material used in this investigation is a 1070 steel which displays a pearlitic microstructure. All data acquisition and control were performed with microcomputers. Two kinds of tests were conducted on both uniaxial solid specimens and biaxial tubular specimens. One is a single step test in which the stress magnitudes are constant during the test. The other is a multiple step test, which is composed of several single step tests. The details of material can be found in an earlier work by Jiang and Sehitoglu (1994a,b) and early references on this class of materials can be found in Slavik and Sehitoglu (1987).

Experimental data for 1070 steel (Jiang, 1993; Jiang and Sehitoglu, 1994a,b) are utilized to examine the new model's capability to predict ratchetting. The uniaxial experiments were conducted using solid circular specimens. The axial-torsion biaxial experiments were conducted employing thin-walled tubular specimens. In the simulations using the new plasticity model, the number of terms for the backstress expansion, M, was 10. Cyclic hardening for 1070 steel is small and is neglected. In Figs. 4 and 5 the experimental ratchetting rates are presented on logarithmic coordinates along with simulations with different values for $\chi^{(i)}$ (i = 1, 2, . . . , 10). The solid lines in Figs. 4 and 5 are obtained from a uniaxial experiment and a nonproportional axial-torsion experiment, respectively. The nonproportional axial-torsion experiment consist of fully reversed shear with superimposed static axial stress. In Fig. 5 the ratchetting in the shear direction is not shown because in this case both the experiment and the predictions demonstrate no shear ratchetting. In both cases, the experimental axial ratchetting rate varies from around 10^{-3} per cycle at the beginning of the loading to on the order of 10^{-6} per cycle after a few thousand cycles. Since the experimental results are approximately a straight line on log-log coordinates, the ratchetting rates follow a power law relation with respect to the loading cycles. Figures 4 and 5 reveal the pronounced influence of the exponents $\chi^{(i)}$ on the ratchetting rate predicted for both proportional and nonproportional loading. The larger the numerical values of the exponents $\chi^{(i)}$ (i = 1, 2, . . . , 10), the faster the models predict ratchetting rate decay. This contrasts with the apparent insensitivity of $\chi^{(i)}$ (i = 1, 2, . . . , 10) previously discussed for the fully reversed strain-controlled uniaxial loading conditions (Fig. 3). When $\chi^{(i)} = 0$ (i = 1, 2, . . . , 10) the model predicts a slight ratchetting rate decay for the first 100 cycles and then constant ratchetting. When $\chi^{(i)} = +\infty$ (i = 1, 2, . . . , 10), no ratchetting is predicted for the uniaxial loading. This is because the model with $\chi^{(i)} = +\infty$ (i = 1, 2, . . . , 10) produces a perfect hysteresis loop closure. For the nonproportional loading consisting of fully reversed shear with constant axial stress (Fig. 5), the model with $\chi^{(i)} = +\infty$ (i = 1, 2, . . . , 10) predicts ratchetting rate decay for about 60 cycles before ratchetting arrest. This confirms that, in the absence of cyclic hardening, the new plasticity model can predict (i) long-term ratchetting rate decay and (ii) ratchetting from near constant rate to zero rate (ratchetting arrest) for both proportional and nonproportional loading.

The exponents $\chi^{(i)}$ (i = 1, 2, . . . , M) in the new model are obtained from the analysis of the single-step uniaxial experimental ratchetting results, and the constants in the expression for $\chi^{(i)}$ (i = 1, 2, . . . , M) are determined via the procedures forwarded previously. These constants are listed in Table 1 for 1070 Steel. The ratchetting predictions using these constants are compared with the experimental results in Figs. 6 through 8. In all the figures solid

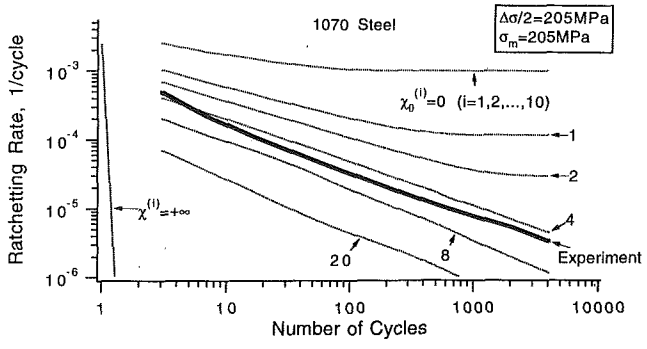

Fig. 4 Relationship between $\chi^{(i)}$ and ratchetting rate predicted by the new model for uniaxial loading

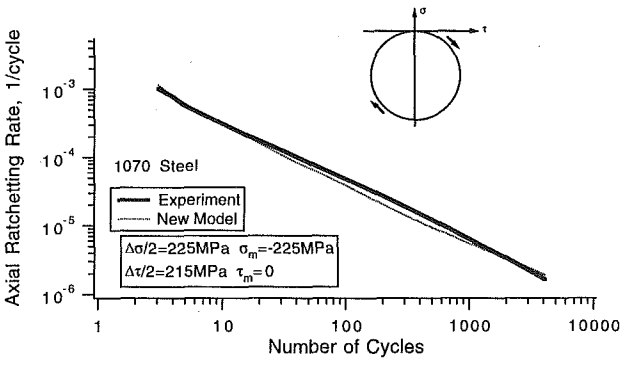

Fig. 6 Comparison of experimental data and axial ratchetting rate predicted by the new model for an "ellipse" shaped axial-torsion loading path (both experiment and new model simulation show no shear ratchetting)

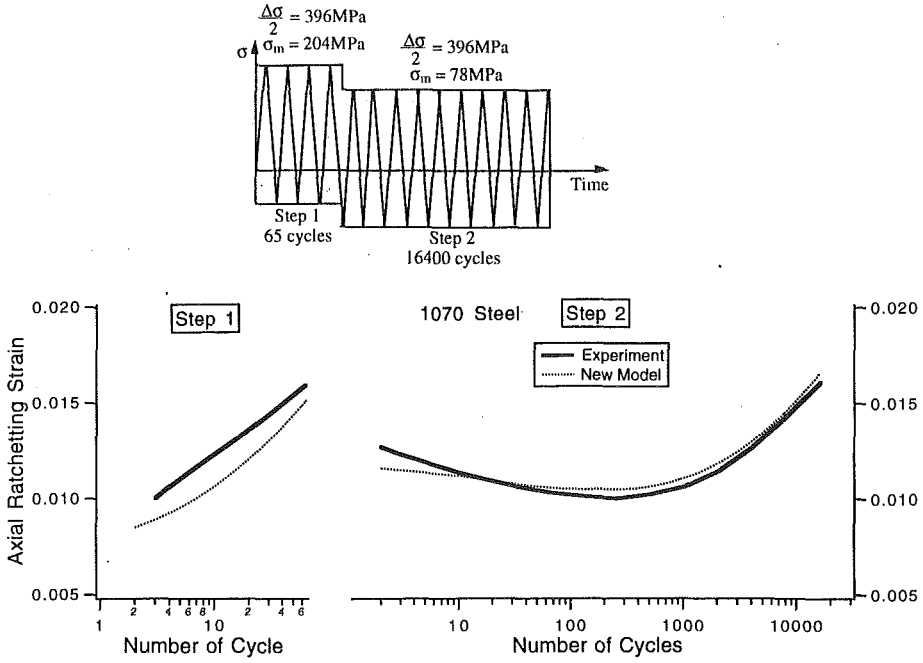

Fig. 7 Comparison of experimental data and ratchetting strain predicted by the new model for a two-step uniaxial loading

lines represent experimental results and dotted lines are predictions obtained using the new plasticity model. Shown in Fig. 6 is the comparison of experimental data and ratchetting rate predicted by the new model for an "ellipse" shaped axial-torsion loading path. The axial ratchetting rate shown is the absolute value because the actual axial ratchetting is in the compressive axial direction. Clearly, the agreement between experiment and simulation is very close for the long loading history. The ratchetting in shear direction is not

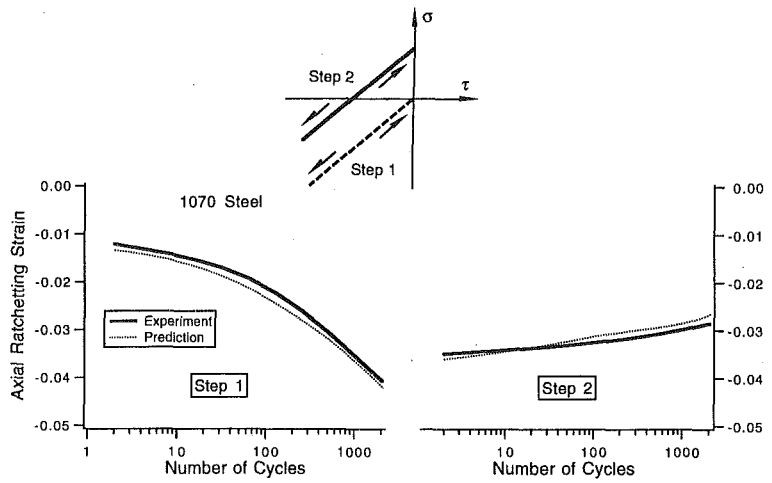

Fig. 8(*a*)

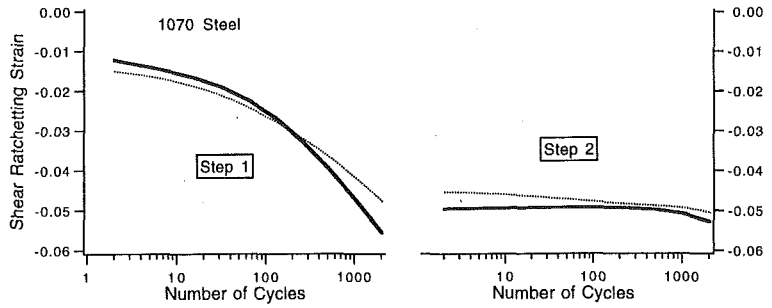

Fig. 8(*b*)

Fig. 8 Comparison of experimental data and ratchetting strain predicted by the new model for a two-step nonproportional loading history; (*a*) ratchetting in the axial direction, (*b*) ratchetting in the shear direction

shown since both the experiment and simulation produces no ratchetting in shear direction.

Figure 7 is a two-step uniaxial loading case. Because of a reduction of mean stress, there is a ratchetting direction change in Step 2. Obviously, the model correlates with the experiment very well. It should be noted that in this case ratchetting strain instead of ratchetting rate is used. The difference between experiment and simulation for Step 1 is mainly contributed by the first few cycles. Notably in Step 2 the model mimics the experimental ratchetting direction change appropriately and the number of loading cycles is up to 2×10^4.

Comparison of experimental data and ratchetting strain predicted by the new model for a two-step loading history is displayed in Fig. 8. Step 1 of this loading history is a axial-torsion proportional loading. In Step 1 there is a compressive mean stress in axial direction and a mean shear stress. In Step 2 the mean axial stress is reduced to zero. Step 2 is nonproportional because the ratio of axial to shear stress changes during the cycle. The axial strain component is shown in Fig. 8(a) and the shear component is presented in Fig. 8(b). Under Step 1, ratchetting rate decays in both axial and shear directions. During Step 2 loading, the axial ratchetting direction is opposite to that of Step 1 and the shear ratchetting rate decreases considerably. From Fig. 8(a), we can find that the model duplicates the experimental axial ratchetting behavior very well. In the shear direction as shown in Fig. 8(b), the agreement between experiment and simulation is not as close as that in the axial direction. This is partly because the shear stress was assumed to be homogeneous despite a small gradient in the radial direction of the thin walled cylinder.

The number of terms for the backstress expansion, M, has a weak influence on the predicted stress-strain responses for balanced loading, but a strong influence on the ratchetting prediction for unbalanced loading (Jiang, 1993). It should be noted that the selection of $M = 10$ in the previous simulations does not imply that the model inherently requires a large number of backstress terms. From the aforementioned discussion, for ratchetting rate predictions, $M = 5 \sim 10$ seems sufficient. Computer simulations for a large number of loading cycles is time consuming when both M and the number of incremental steps for a loading cycle increase. Compromises have to be made between the accuracy of the prediction and the number of loading cycles simulated. It is suggested that detailed ratchetting predictions be made for a limited number of loading cycles, and the results be extrapolated for longer loading histories using a power relation between the ratchetting rate and number of loading cycles (Jiang, 1993).

For single step loading, each $\chi^{(i)}$ has a significant influence on the predicted ratchetting rate for a limited range of loading cycles. The exponents $\chi^{(i)}$ with small i's have strong control over the initial ratchetting rate, and a weak influence on the long term ratchetting. The exponents $\chi^{(i)}$ with large i's on the other hand control the ratchetting predicted for a large number of loading cycles at a given stress level. The relationship between the ratchetting rate predicted and the selection of the exponents $\chi^{(i)}$ illustrates how the exponents $\chi^{(i)}$ ($i = 1, 2, \ldots, M$) would be selected. Detailed discussions can be found in Jiang (1993).

3 Further Discussion on Ratchetting

We attempt to gain further insight into the ratchetting phenomenon here. Deriving the ratchetting increment per cycle in closed form for nonproportional loading is virtually impossible. However, it may be helpful to discuss a cyclically stable unbalanced uniaxial simulation. An arbitrary stress-strain response is schematically shown in Fig. 9 for a uniaxial loading. Point 1 denotes the beginning of the cycle, and the material is stressed in the forward direction to 2. At point 2, the material is unloaded until the stress 3 is reached.

The ratchetting rate (ratchetting strain per cycle) for this case is

$$\frac{d\epsilon_r}{dN} = \sum_{i=1}^{M} \frac{d\epsilon_r^{(i)}}{dN} = \int_1^3 d\epsilon^p \tag{16}$$

where

$$\frac{d\epsilon_r^{(i)}}{dN} = \frac{c^{(i)} r^{(i)} \left[\int_1^2 \left(\frac{\|\boldsymbol{\alpha}^{(i)}\|}{r^{(i)}} \right)^{\chi^{(i)}+1} \mathbf{L}^{(i)} : \mathbf{n} d\epsilon^p + \int_2^3 \left(\frac{|\boldsymbol{\alpha}^{(i)}|}{r^{(i)}} \right)^{\chi^{(i)}+1} \mathbf{L}^{(i)} : \mathbf{n} d\epsilon^p \right]}{\sum_{j=1}^{M} c^{(j)} r^{(j)}} \quad (i = 1, 2, \ldots, M). \tag{17}$$

The term, $d\epsilon_r^{(i)}/dN$, in the previous equations represents the contribution to ratchetting rate by the variation of an individual backstress. A few insights can be gained from the examination of Eq. (17). The denominator on the right side of Eq. (17) is a constant since a cyclically stable material was assumed. If $\boldsymbol{\alpha}^{(i)}$ varies symmetrically (i.e., no mean value), the integral on the right-hand side of Eq. (17) will be zero, which results in $d\epsilon_r^{(i)}/dN = 0$. The quantity $(\|\boldsymbol{\alpha}^{(i)}\| r^{(i)})^{\chi^{(i)}+1}$ is equal to or less than 1.0. Therefore, if $\chi^{(i)} = +\infty$, then $d\epsilon_r^{(i)}/dN = 0$. For balanced loading, the scalar product of vector, $\mathbf{L}^{(i)}$ and $\mathbf{n}$ will change sign for loading from 1 to 2 and 2 to 3 (refer to Fig. 9) and results in the sum of these integrals to be approximately zero, i.e., $d\epsilon_r^{(i)}/dN \approx 0$. For a single step, fully reversed uniaxial loading, all the backstresses vary symmetrically and no ratchetting is predicted.

Figure 10 shows a two-step unbalanced uniaxial loading. For the one-dimensional problem of tension-compression, $\boldsymbol{\alpha}^{(i)}$ can be represented by the value of the component $\alpha_{11}^{(i)}$. The term, $\sqrt{\frac{3}{2}}\alpha_{11}^{(i)}/r^{(i)}$, is a normalized quality representing the backstress $\boldsymbol{\alpha}^{(i)}$ for the uniaxial case. In Fig. 10 the number of terms for the backstress, M, is 5 since the desire is to qualitatively display the behavior of $\boldsymbol{\alpha}^{(i)}$. The selection of the material constants does not qualitatively alter the ensuing points of discussion. The predicted ratchetting rates for both steps are shown in Fig. 10(b), and the variations of the backstresses with the loading history are presented in Fig. 10(c). During Step 1 loading, ratchetting rate decay is predicted. The corresponding variations

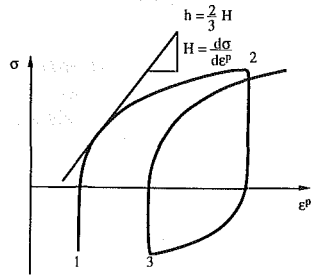

Fig. 9 Schematic representation of strain ratchetting for a uniaxial simulation

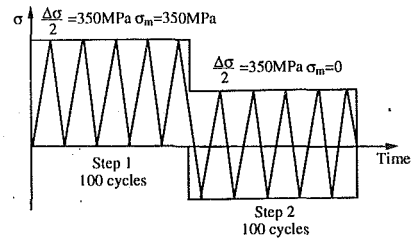

Fig. 10(*a*)

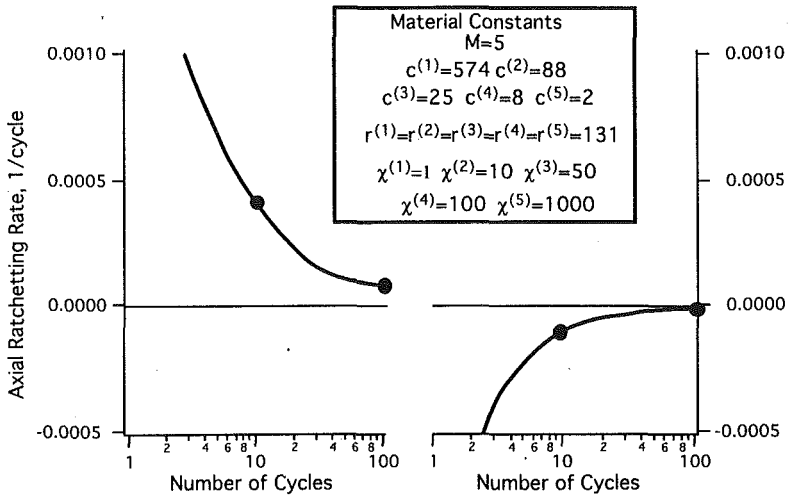

Fig. 10(*b*)

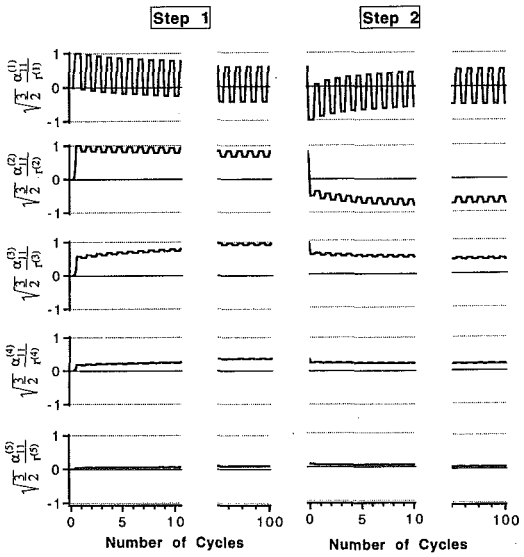

Fig. 10(*c*)

Fig. 10 Demonstration of ratchetting rate decay predicted by the new model for a two-step uniaxial loading; (*a*) two-step uniaxial loading, (*b*) ratchetting rate, (*c*) $\alpha_{11}^{(i)}$ variations with loading cycles

of the backstresses shown on the left side of Fig. 10(*c*) are responsible for the ratchetting rate decay. The magnitudes of backstress variations are in an order consistent with the size of $c^{(i)}$ ($i = 1, 2, 3, 4, 5$). Subsequently, the mean values of $\alpha_{11}^{(1)}$ and $\alpha_{11}^{(2)}$ saturate to zero with increasing cycles and the mean values of $\alpha_{11}^{(4)}$ and $\alpha_{11}^{(5)}$ increase at the same time. The amplitudes of the backstresses do not change with loading cycles. According to Eq. (17), for the same variation of the backstress and $\chi^{(i)}$, a larger value of $c^{(i)}r^{(i)}$ will result in a larger ratchetting rate. Because it was assumed that $r^{(1)} = r^{(2)} = r^{(3)} = r^{(4)} = r^{(5)}$, a larger $c^{(i)}$ results in a larger $c^{(i)}r^{(i)}$. The decrease of the mean values of $\alpha_{11}^{(1)}$ and $\alpha_{11}^{(2)}$ (corresponding to larger $c^{(i)}r^{(i)}$ values) mainly contributes to the initial ratchetting rate decay predicted. It should be noted that the mean value of the total backstress is proportional to the mean stress of the stress-controlled uniaxial loading cycle. Therefore, the sum of all the backstress has a fixed mean value for a given step in the loading. The decrease in the mean values of $\alpha_{11}^{(1)}$ and $\alpha_{11}^{(2)}$ is consistent with the increase of the mean values of $\alpha_{11}^{(4)}$ and $\alpha_{11}^{(5)}$. It is this shifting of the mean values of the backstresses in combination with the smaller amplitude of $\alpha_{11}^{(4)}$ and $\alpha_{11}^{(5)}$ that contributes to the continued ratchetting rate decay.

When the mean stress is zero in Step 2, the model predicts ratchetting in the direction opposite to that in the first step. From the right side of Fig. 10(*b*), the ratchetting rate (absolute value) also decreases with increasing number of loading cycles, which again can be explained by the variations of the backstresses (refer to the right side of Fig. 10(*c*)). When Step 2 with a different mean stress begins, there are sudden changes in the backstresses, which corresponds to a change in the ratchetting rate. The backstresses $\alpha_{11}^{(1)}$ and $\alpha_{11}^{(2)}$ with initial negative mean levels contribute to the ratchetting rate in the negative direction, while the other three backstress parts with positive mean values produce ratchetting in the positive direction. As was previously stipulated, a larger amplitude of a backstress contributes more to the ratchetting rate, hence the overall ratchetting rate is negative. Since the mean stress in Step 2 is zero, all the mean values of the backstresses will approach to zero with increasing number of loading cycles. As a result, the ratchetting rate decreases with increasing number of cycles. For ratchetting under nonproportional loading, the ratchetting predicted using the new model may be explained in a similar way. However, for nonproportional loading, the ratchetting rate is not only dependent on the variations of the backstresses but also on the variations of $\mathbf{L}^{(i)} : \mathbf{n}$ ($i = 1, 2, \ldots, M$). A straightforward illustration is more difficult for unbalanced nonproportional loading.

4 Conclusions

The following conclusions are drawn from the work:

1 The new plasticity model was applied to the ratchetting predictions of 1070 steel. Its capability to improve long-term ratchetting and multiple step ratchetting predictions was demonstrated.

2 The material constants in the new plasticity model can be divided into two independent groups; one group, $c^{(i)}$ and $r^{(i)}$ ($i = 1, 2, \ldots, M$), which describes balanced loading and the other group, $\chi^{(i)}$ ($i = 1, 2, \ldots, M$), which characterizes unbalanced loading. The independence of the two groups of material constants and the interpretation of the model with a limiting surface concept facilitated the determination of material constants.

3 The material displays minimal cyclic hardening, however, non-Masing behavior is observed. The model correlated the non-Masing behavior accurately.

4 For multiple step loading, the material exhibits a memory of the previous loading history. Due to this memory effect the strain ratchetting may accelerate under certain circumstances, although such an acceleration in ratchetting rate is short-lived. The model predicts the prior loading history effect on the subsequent ratchetting, the change in ratchetting direction and the dissipation of this effect with increasing number of loading cycles.

Acknowledgments

Professor Sehitoglu acknowledges the financial support from Department of Energy, Basic Energy Sciences, DOE DEFG02-93ER14393. The continued support of Association of American Railroads, Technical Center, Chicago, IL and the encouragement of Dr. Dan Stone, AAR, are also acknowledged.

References

Slavik, D., and Sehitoglu, H., 1987, "A Constitutive Model for High Temperature Loading, Part I—Experimentally Based Form of the Equations," *Thermal Stress, Material Deformation, and Thermo-mechanical Fatigue,* ASME, New York, PVP-123, pp. 65–73.

Slavik, D., and Sehitoglu, H., 1987, "A Constitutive Model for High Temperature Loading, Part II—Comparisons of Simulations with Experiments," *Thermal Stress, Material Deformation, and Thermo-mechanical Fatigue,* ASME, New York, PVP-123, pp. 75–82.